COBEM 2021 26th International Congress of Mechanical Engineering
November 22-26, 2021, Virtual Congress, Brazil

COB-2021-0324
NUMERICAL PREDICTIONS OF THE LIQUID FILM THICKNESS FOR GAS-LIQUID FLOWS ON SEPARATED PATTERN

Vinicius Sylvestre Simm*
Luiz Eduardo Muzzo†
Luiz Eduardo Melo Lima‡
Department of Mechanics, Federal University of Technology—Paraná—, Ponta Grossa, PR 84017-220, Brazil
*viniciussimm@alunos.utfpr.edu.br, †luizeduardomuzzo@gmail.com, ‡lelima@utfpr.edu.br

Abstract. *Multiphase flows occur in various industry branches, as seen in power plants, nuclear reactors, and oil and gas production. Several flow patterns arise according to the spatial distribution of the phases, which depend on flow rates, physical properties of the fluids, and geometrical characteristics of the pipe. Stratified and annular flows constitute an important two-phase flow pattern in ducts, called separated (or separated phases) flow, which has a variety of practical applications, for example, the core flow. For gas-liquid flows, this pattern presents itself as a liquid film in contact with the pipe wall flowing parallel with a gas core that can drag liquid droplets. In horizontal flows, the interface is flat. But with the increase in gas velocity, waves appear at the interface, the gas core drags the liquid droplets, and the film "scales" the walls, tending to form an eccentric annular pattern. On the other hand, a concentric annular pattern appears in vertical flows. The experimental determination of the film thickness is difficult and limited. Therefore, the mathematical models based on the physical aspects of the phenomenon are developed and employed for this parameter estimation. These models are dependent on several parameters, such as the entrainment fraction of the droplets, for example, which depends on the atomization and deposition rates of these droplets, and is often modeled through empirical correlations. In the present work, the influence of droplets entrainment fraction and interfacial friction factor on the film thickness prediction was evaluated. To this end, a computational code was developed to solve the implicit equation of the film model. The results obtained for the film thickness were compared with two experimental literature databases: one for horizontal stratified and the other for vertical annular. It was possible to identify the precision of the droplets entrainment fraction correlations analyzed from the obtained deviations. The gas-liquid ratio influences the correlations for entrainment fraction of droplets, and the correlations for interfacial friction factor are dependent on flow pattern (stratified and annular).*

Keywords: *multiphase flow, liquid film thickness, modeling.*

1. INTRODUCTION

Multiphase flows occur in many industrial sectors, for example, power plants, chemical processes, refrigeration cycles, and the oil industry. Stratified and annular flows are two-phase flow patterns usually found in pipes (Torres, 1992), where a liquid film flows in contact with the pipe wall, and a gas phase flows in the core (pipe center), separated by a well-established interface. Among other characteristics, the thickness of the film is relevant to understand the effects of corrosion and erosion in a pipeline (Oliemans *et al.*, 1986). Stratified flows are found in natural gas pipelines, where heavier hydrocarbons condense and display a flat and approximately smooth surface at slow velocities. As the core velocity increases, waves might appear, and the film may climb through the wall, showing an annular pattern. Due to the limitations of empirical methods to precisely analyze the two-phase flow pattern, analytical methods have been created guided by the physic aspect of the problem.

Pedras (1993) studied the stratified flow and related the core velocity with the formation of waves on the film surface. For constant liquid velocity, it was noticed a notable change in the interface as the gas flow rate increases: large waves moved across the contact interface between the gas and the liquid phases. As velocity further increased, the film thickness decreased, as did wave sizes and their frequency. This occurs because part of the liquid is carried by the core in the form of droplets, which arise from the breaking of wave crests. Such droplets enter the core at a velocity slower than the medium and are accelerated by it. When they return to the film, the droplets suffer a deceleration. A decrease in core turbulence occurs when droplets are found in the core, and the wall shear stress increases from 15% to 50% due to droplets deposition on the film. Hanratty (1991) lessons that the presence of droplets can change the turbulence of the core and influence the transfer of momentum between gas and liquid when they collide with the film. Furthermore, such droplets contribute from 0% to 20% to the interfacial tension. Li *et al.* (2013) suggested the presence of gas bubbles in the film, just as liquid droplets are found in the gaseous core.

Studies on film thickness have been covered by Li *et al.* (2013) and Oliemans *et al.* (1986), among others. Li *et al.* (2013) developed a model to predict pressure loss and film thickness in horizontal two-phase flow of a non-Newtonian fluid, which also takes into account droplets' drag and film aeration effects. Some initial conditions were assumed in their model: the film is laminar, and the core is turbulent; the film is symmetrical; film and core have the same pressure gradient in the flow direction; pressure gradients are considered null in the radial direction; the core velocity is the sum of the interfacial velocity and the turbulence component; the core/film interface is regular; there is no slipping between the tube wall and the film, as between the liquid and the gas phases; the effects of gravity acceleration are disregarded; the densities of gas and non-Newtonian liquid are constant. The film thickness obtained by the model showed a 10% deviation concerning the experimental data from the literature.

Oliemans *et al.* (1986) studied pressure drop, film thickness, and droplets drag in a vertical two-phase annular flow, with a film on the tube walls and a gaseous core containing droplets in the center of the tube. The considerations assumed in their model are: one-dimensional, steady-state, ascending, and concurrent flow with axial symmetry; no interfacial mass transfer; the acceleration term is neglected in the total pressure gradient; densities, dynamic viscosities, and surface tension of the phases are considered constant; the superficial velocities of gas and liquid are given; the droplets have the same velocity as the gas (homogeneous flow). In this model, it was not possible to distinguish the frictional contribution of gas and droplets being atomized or deposited on the film, and pressure drop, film thickness, and droplets' drag can be obtained simultaneously.

In the present work, a numerical model was assembled with well-established separated flow equations to estimate the film thickness in gas-liquid flows. Said model was implemented in computational code written in MATLAB® language. The influences of two parameters for film thickness estimation were analyzed: the interfacial friction factor and the entrainment fraction of the droplets. Correlations for these two parameters from the literature were applied on the computational code, especially for the entrainment fraction of the droplets for which five correlations were tested. Experimental data from the literature on stratified horizontal and vertical annular flows were compared against the results to verify the developed numerical model.

2. MODEL

The separated gas-liquid flow consists of two distinct (continuous) phases or components flowing concurrently, separated by a well-defined interface. In stratified flow, the liquid phase flows at the bottom of the pipe and the gas phase at the top of it. When a pipeline is horizontal or approximately horizontal, and the flow velocity is small, the interface between the phases is approximately smooth. This interface may acquire a wavy characteristic and scale the walls of the pipeline as the tube inclination or flow velocity increases. When this phenomenon reaches proportions in which the liquid surrounds the entire wall of the pipe, the flow becomes annular. The two distinct regions of separated gas-liquid flow consist of a liquid film, which tends to stay attached to the pipe wall, and a gaseous core, which may contain droplets of the liquid phase, resulting from atomization and deposition processes. The interface between film and core may be flat, for stratified flows, or concentric, when the flow pattern is annular (Lima, 2011). However, some models also consider the occurrence of an eccentric interface.

The developed numerical model considers a separated flow flowing in a pipe of diameter D, perimeter S, cross-sectional area A, absolute roughness ε, and inclined by an angle θ. Table 1 shows equations for the following geometric properties: film ϕ_f and core ϕ_c fractions, film S_f and core S_c wetted perimeters, interfacial perimeter S_i, cross-sectional area occupied by the film A_f and by the core A_c, film D_f and core D_c hydraulic diameters. The angle formed by the flat interface concerning the center of the tube is represented by $\lambda_i = 2\arccos(1-2\delta_f)$, and $\delta_f = H_f/D$ represents the dimensionless film thickness, where H_f is the film thickness.

Table 1. Equations for the geometric properties of separated flow according to the interface shape.

Geometric property	Interface shape	
	Flat $(0 < \delta_f < 1)$	Concentric $(0 < \delta_f < 0.5)$
ϕ_f	$(\lambda_i - \sin\lambda_i)\,/\,(2\pi)$	$4\delta_f\,(1-\delta_f)$
ϕ_c	$1-\phi_f$	$1-\phi_f$
S_f	$\lambda_i/\,(2\pi)$	S
S_c	$S - S_f$	0
S_i	$S\sin\left(\lambda_i/2\right)/\pi$	$S\,(1-2\delta_f)$
A_f	$\phi_f A$	$\phi_f A$
A_c	$\phi_c A$	$\phi_c A$
D_f	$4A_c/\,(S_c+S_i)$	$4A_c/\,(S_c+S_i)$
D_c	$4A_f/S_f$	$4A_f/S_f$

In a separated flow, the phases flow with a certain absolute velocity, U_c for the core and U_f for the film, and a relative velocity between the phases defined as $V_r = U_c - U_f$. U_c and U_f are given by Eqs. (1) and (2), respectively.

$$U_c = \left(J_g + E_d J_l\right)/\phi_c \tag{1}$$

$$U_f = \left(J_l - E_d J_l\right)/\phi_f \tag{2}$$

Where J_g and J_l are the superficial velocities of the gas and liquid phases, respectively, and E_d is the droplets entrainment fraction.

The densities ρ_c and ρ_f, and the dynamic viscosities μ_c and μ_f of the core and film, respectively, are defined according to the Tab. 2.

Table 2. Equations for the physical properties of the phases.

Physical	Phase	
property	Core ($k = c$)	Film ($k = f$)
ρ_k	$\phi_{gc}\rho_g + \phi_d\rho_l$	ρ_l
μ_k	$\phi_{gc}\mu_g + \phi_d\mu_l$	μ_l

Where ρ_g is the density of the gas phase, ρ_l is the density of the liquid phase, $\phi_{gc} = 1 - \phi_d$ is the fraction of gas in the core, and ϕ_d is the fraction of droplets in the core, which is defined from the superficial velocities of the gas and liquid phases and by the droplets entrainment fraction, as shown in Eq. (3).

$$\phi_d = \frac{J_l E_d}{J_g + J_l E_d} \tag{3}$$

In steady-state and away from the film formation area, the atomization and deposition rates of the droplets are approximately equal, such that the droplets entrainment fraction E_d is locally in equilibrium. In this situation, it can be estimated from empirical correlations or simplified physical models available in the literature. However, these correlations suffer from the imprecision of the experimental data and the lack of a consistent physical model. Correlations for estimating E_d generally depend on characteristics of the pipe, as well as the flow rates and physical properties of the phases, and are often expressed in terms of dimensionless numbers. Table 3 shows five correlations for the droplets entrainment fraction selected from the literature.

Table 3. Correlations for the droplets entrainment fraction E_d.

Correlation	E_d	Author
C1	$1 - \exp\left[-0.125\left(10^4 \frac{\mathrm{We}_g}{\mathrm{Re}_g}\sqrt{\frac{\rho_g}{\rho_l}} - 1.5\right)\right]$	Wallis (1969)
C2	$\frac{\Omega}{1+\Omega}$	Oliemans *et al.* (1986)
C3	$\tanh\left(7.25 \times 10^{-7}\mathrm{Re}_l^{1/4}\widehat{\mathrm{We}}_g^{5/4}\right)$	Ishii and Mishima (1989)
C4	$\left(1 - \frac{\mathrm{Re}_{lmin}}{\mathrm{Re}_l}\right)\tanh\left(2.31 \times 10^{-4}\mathrm{Re}_l^{-0.35}\widetilde{\mathrm{We}}_g^{5/4}\right)$	Sawant *et al.* (2008)
C5	$\left(1 - \frac{\widehat{\mathrm{Re}}_{lmin}}{\mathrm{Re}_l}\right)\tanh\left(2.31 \times 10^{-4}\mathrm{Re}_l^{-0.35}\widetilde{\mathrm{We}}_g^{5/4}\right)$	Sawant *et al.* (2009)

The parameters shown in the equations from Tab. 3 are defined next. The Reynolds numbers of the gas Re_g and liquid Re_l phases, as well as the Weber number of the gas phase We_g are defined by Eqs. (4), (5), and (6), respectively.

$$\mathrm{Re}_g = J_g D/\nu_g \tag{4}$$

$$\mathrm{Re}_l = J_l D/\nu_l \tag{5}$$

$$\mathrm{We}_g = J_g^2 D\rho_g/\sigma \tag{6}$$

Where ν_g and ν_l are the kinematic viscosities of the gas and liquid phases, respectively, while σ the gas-liquid surface tension. The minimum liquid Reynolds numbers Re_{lmin} and $\widehat{\mathrm{Re}}_{lmin}$ are defined by Eqs. (7) and (8), respectively.

$$\mathrm{Re}_{lmin} = 250\log\mathrm{Re}_l - 1265 \tag{7}$$

$$\widehat{\mathrm{Re}}_{lmin} = 13/\sqrt{N_\mu} + 0.3\left(\mathrm{Re}_l - 13/\sqrt{N_\mu}\right)^{0.95} \tag{8}$$

Where N_μ is the dimensionless number of viscosity, defined by the Eq. (9), $\Delta\rho = \rho_l - \rho_g$ being the difference between densities of the liquid and gas phases.

$$N_\mu = \mu_l \left(\frac{g\Delta\rho}{\rho_l^2 \sigma^3} \right)^{1/4} \tag{9}$$

The modified gas Weber numbers $\widehat{\mathrm{We}}_g$ and $\widetilde{\mathrm{We}}_g$ are defined by the Eqs. (10) and (11), respectively.

$$\widehat{\mathrm{We}}_g = \mathrm{We}_g \left(\frac{\Delta\rho}{\rho_g} \right)^{1/3} \tag{10}$$

$$\widetilde{\mathrm{We}}_g = \mathrm{We}_g \left(\frac{\Delta\rho}{\rho_g} \right)^{1/4} \tag{11}$$

In addition, there is the dimensionless parameter Ω, which is defined by Eq. (12).

$$\Omega = 10^{-2.52} J_g^{1.44} J_l^{0.7} \rho_g^{0.18} \rho_l^{1.08} \mu_g^{0.28} \mu_l^{0.27} \sigma^{-1.8} g^{0.46} D^{1.72} \tag{12}$$

In stratified flow, both the gaseous core and the liquid film exert shear stresses on the pipe walls. There is also interfacial shear stress between the two phases. In annular flow, shear stresses occur between the film and the pipe wall and at the gas-liquid interface, as the core flows only in the center of the pipe. The core τ_c and film τ_f shear stresses are defined by Eq. (13) in terms of the Fanning friction factor, where $k = c$ for the core and $k = f$ for the film.

$$\tau_k = \frac{1}{2} C_{fk} \rho_k U_k \left| U_k \right| \tag{13}$$

The Fanning friction factor may be obtained by the Hagen–Poiseuille law for the laminar regime or by correlation proposed by Haaland (1983) for the turbulent regime, according to the Eq. (14).

$$C_{fk} = \begin{cases} \frac{16}{\mathrm{Re}_k} & \text{if laminar flow} \\ \left[-3.6 \log \left(\left\{ \frac{\varepsilon}{3.7 D_k} \right\}^{1.11} + \frac{6.9}{\mathrm{Re}_k} \right) \right]^{-2} & \text{if turbulent flow} \end{cases} \tag{14}$$

The interfacial shear stress τ_i is defined analogously by Eq. (15) but in terms of the relative velocity $V_r (= U_c - U_f)$.

$$\tau_i = \frac{1}{2} C_{fi} \rho_c V_r \left| V_r \right| \tag{15}$$

Where the interfacial friction factor C_{fi} depends on the shape of the interface, flat or concentric, according to Tab. 4.

Table 4. Correlations for the interfacial friction factor C_{fi} as a function of interface shape.

Interface shape	C_{fi}	Criterion	Author
Flat	0.014	$J_g \leq 15$ m/s	Cohen and Hanratty (1968)
	$0.0625 \left[\log \left(\frac{15}{\mathrm{Re}_c} + \frac{2{,}3\delta_f}{3{,}715} \right) \right]^{-2}$	$J_g > 15$ m/s	Hart *et al.* (1989)
Concentric	$C_{fc} \left(1 + 300\delta_f \right)$	$D^* \leq 2$	Wallis (1969)
	$C_{fs} \left(1 + \frac{0.3\delta_f^{0.12} \mathrm{Re}_g^{0.54}}{\mathrm{Fr}_g^{6/5}} \right)^{3/2}$	$D^* > 2$	Aliyu *et al.* (2017)

In the correlations shown in Tab. 4, $D^* = \sqrt{\mathrm{Eo}}$ is the dimensionless hydraulic diameter, and $C_{fs} = 0.046 \mathrm{Re}_g^{0,2}$ is a dimensionless fit parameter defined by Aliyu *et al.* (2017). Eötwös number Eo, gas Froude number Fr_g, and core Reynolds number Re_c are defined by Eqs. (16), (17), and (18), respectively.

$$\mathrm{Eo} = g D^2 \Delta\rho / \sigma \tag{16}$$

$$\mathrm{Fr}_g = J_g / \sqrt{gD} \tag{17}$$

$$\mathrm{Re}_c = U_c D / \nu_c \tag{18}$$

Where $\nu_c = \phi_{gc} \nu_g + \phi_d \nu_l$ is the kinematic viscosity of the core.

With all the parameters previously depicted, it is possible to calculate the film thickness H_f by the solution of the implicit function defined by Eq. (19). The set of equations presented in this section establish the numerical model to solve for the film thickness in separated (stratified or annular) gas-liquid flows.

$$f(H_f) = \frac{\tau_c S_c}{A_c} - \frac{\tau_f S_f}{A_f} + \tau_i S_i \left(\frac{1}{A_c} + \frac{1}{A_f} \right) - (\rho_f - \rho_c) g \sin\theta = 0 \tag{19}$$

2.1 Solution procedure

To solve the numerical model presented in this work, it is necessary to employ a numerical method of solving nonlinear equations, for example, the bisection method. Equation (19) is implicit in δ_f, so it must be calculated iteratively until the convergence criterion is achieved. The convergence criterion of the bisection method was a residual smaller than 10^{-6}. Figure 1 shows the steps to be taken to implement the numerical model to solve for the film thickness in separated gas-liquid flows.

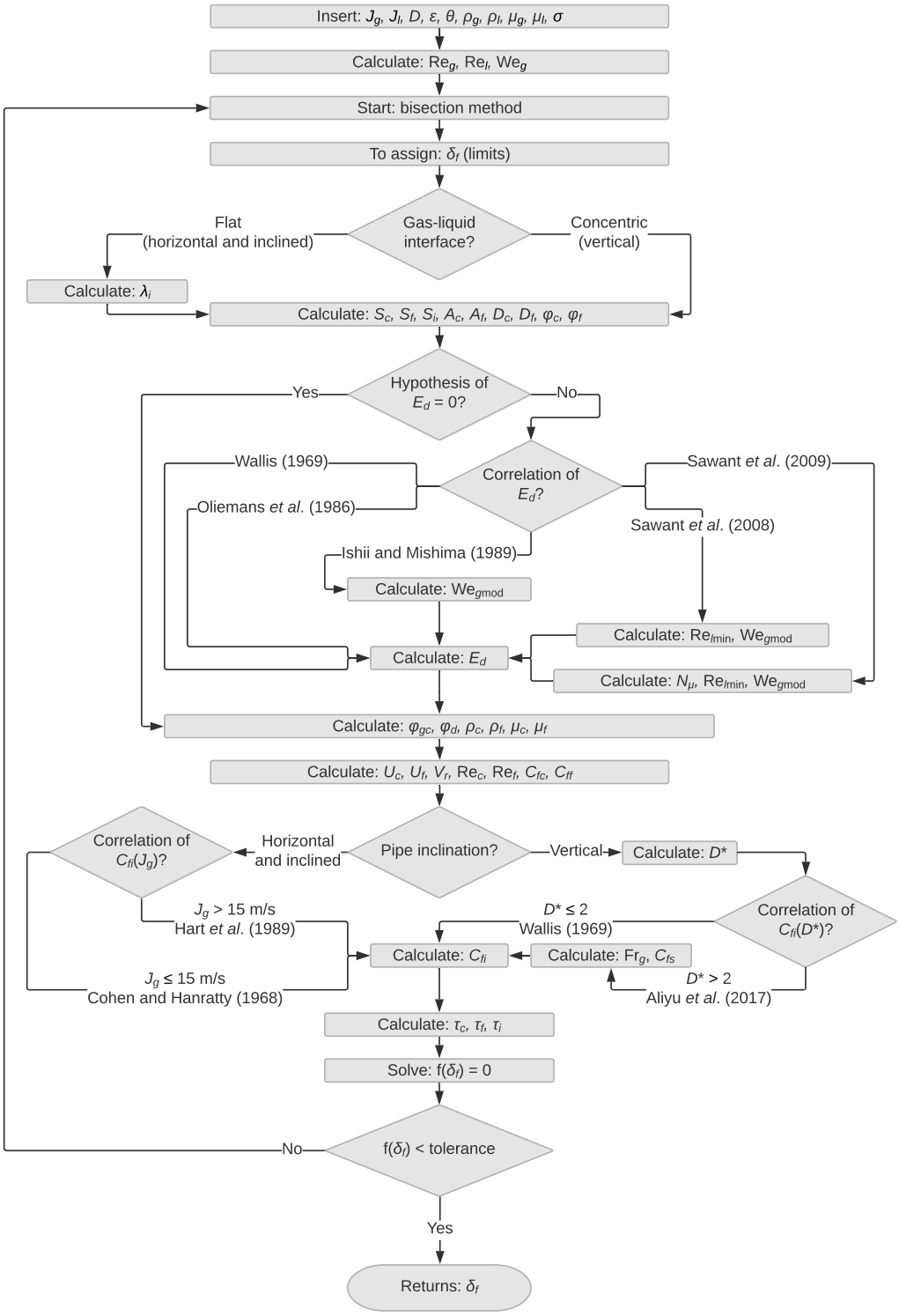

Figure 1. Flowchart for implementation of the numerical model for estimating the film thickness in separated gas-liquid flows.

3. EXPERIMENTAL DATA

To verify the results obtained with the numerical procedure, it is necessary to compare them against experimental film thickness data, which were obtained by Torres (1992) and Aliyu *et al.* (2017). The former used air and water in a horizontal pipe of 38.1 mm internal diameter with temperature and pressure values at conditions close to the standard atmosphere. The air superficial velocities ranged from 4.5 m/s to 25.0 m/s, and from 0.01 m/s to 0.07 m/s for the water phase, obtaining the stratified pattern (Torres, 1992). In the work by Aliyu *et al.* (2017), air-water vertical flow data in the annular pattern were obtained in a pipe with an internal diameter of 101.6 mm and 20 m in length, with temperature and pressure values under conditions close to the standard atmosphere. The superficial velocities of gas and liquid ranged from 11 m/s to 29 m/s and from 0.1 m/s to 1 m/s, respectively. Their results are summarized in Tab. 5.

Table 5. Experimental data compared against the numerical model results.

Stratified pattern by Torres (1992)					Annular pattern by Aliyu *et al.* (2017)				
Test	P	J_l	J_g	H_f	Test	$10^{-5}P$	J_l	J_g	H_f
[#]	[Pa]	[m/s]	[m/s]	[mm]	[#]	[Pa]	[m/s]	[m/s]	[mm]
1	95039.43	0.0088	4.5	2.882	1	1.09	0.1	18.39	1.2
2	94985.29	0.0088	9.3	2.154	2	1.13	0.1	23.66	1.0
3	94647.92	0.0088	12.1	1.512	3	1.15	0.1	28.87	0.7
4	95461.93	0.0106	16.8	0.968	4	1.10	0.2	12.08	1.2
5	95845.72	0.0128	20.5	0.788	5	1.14	0.2	17.51	1.2
6	95859.04	0.0114	25.1	0.496	6	1.18	0.2	22.41	1.0
7	95439.94	0.0209	4.5	5.040	7	1.23	0.2	26.90	1.0
8	95411.31	0.0209	9.3	3.385	8	1.13	0.3	11.70	1.3
9	95532.46	0.0209	12.3	2.187	9	1.18	0.3	16.74	1.1
10	95510.70	0.0190	16.7	1.351	10	1.23	0.3	21.33	1.0
11	96013.59	0.0203	20.6	1.058	11	1.29	0.3	25.47	0.9
12	96032.09	0.0213	24.9	0.709	12	1.17	0.5	11.16	1.2
13	95329.97	0.0295	4.4	6.072	13	1.25	0.5	15.63	1.1
14	95440.24	0.0299	9.5	3.773	14	1.32	0.5	19.62	1.0
15	95549.82	0.0299	12.2	2.609	15	1.40	0.5	22.87	1.0
16	95559.43	0.0287	16.7	1.778	16	1.23	0.7	10.50	1.1
17	95692.66	0.0306	20.6	1.443	17	1.33	0.7	14.45	1.1
18	96249.02	0.0305	24.9	0.915	18	1.42	0.7	17.91	1.0
19	95431.99	0.0397	4.5	6.813	19	1.53	0.7	20.59	0.9
20	95156.38	0.0396	9.4	4.203	20	1.32	1.0	9.65	1.2
21	95287.67	0.0396	12.3	3.061	21	1.44	1.0	13.15	1.1
22	95616.24	0.0411	16.4	2.183	22	1.56	1.0	15.98	1.0
23	96075.93	0.0406	20.7	1.648	23	1.67	1.0	18.56	0.9
24	96365.30	0.0402	25.0	1.108					
25	95256.39	0.0711	4.5	9.279					
26	95441.82	0.0712	9.4	5.264					
27	95588.23	0.0718	12.2	4.017					
28	95746.18	0.0721	16.4	3.116					
29	96342.49	0.0724	20.8	2.410					
30	96686.02	0.0724	25.1	1.668					

For all 53 tests shown in Tab. 5, the numerical model was solved individually with all five correlations for the droplets entrainment fraction that were presented in this work and also for the simplified case where E_d is set to zero. The input data for pipes and phases properties were as follow: absolute pipe roughness $\varepsilon \approx 0$ m, air properties $\rho_g = 1.18$ kg/m^3 and $\mu_g = 1.84 \times 10^{-5}$ Pa s, water properties $\rho_l = 997$ kg/m^3 and $\mu_g = 8.9 \times 10^{-4}$ Pa s, and gas-liquid surface tension $\sigma = 7.197 \times 10^{-2}$ N/m, them being evaluated at temperature and pressure values under conditions close to the standard atmosphere.

3.1 Comparison method

The precision of δ_f values calculated by the numerical model was based on the average value of the absolute relative deviations $\bar{\epsilon}$ between the set experimental data and the calculated values, according to Eq. (20).

$$\bar{\epsilon} = \frac{1}{N} \sum \left| \frac{\delta_{fcalc.} - \delta_{fmeas.}}{\delta_{fmeas.}} \right| \tag{20}$$

The standard deviations σ_ϵ of the absolute relative deviations were also calculated according to Eq. (21), N is the number of experimental tests carried out, which is 30 for the cases of stratified flow and 23 for the cases of annular flow.

$$\sigma_\epsilon = \sqrt{\frac{\sum (\epsilon - \bar{\epsilon})^2}{N - 1}} \tag{21}$$

The numerical model, defined by Eq. (19), and other auxiliary variables of the model as well as the procedure to calculate, presented in Fig. 1, and verify the model against experimental data, using Eqs. (20) and (21), were implemented using a computational code written in the MATLAB® language.

4. RESULTS AND DISCUSSION

Figure 2 shows the comparison of the numerically calculated values of the dimensionless film thickness δ_f, in the ordinate axis, with those experimentally measured, in the abscissa axis, as a function of each of the correlations for droplets entrainment fraction E_d shown in Tab. 3.

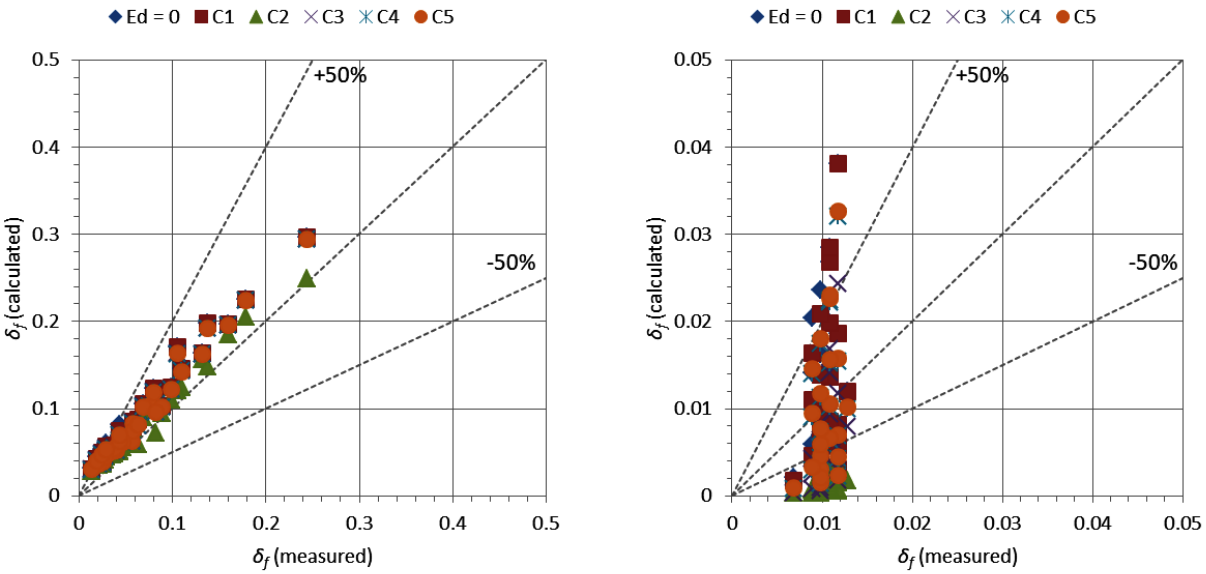

(a) (b)

Figure 2. Comparison of the dimensionless film thickness values δ_f calculated by the numerical model, in the ordinate axis, against experimentally measured values, in the abscissa axis, by Torres (1992) (a) e Aliyu *et al.* (2017) (b). The correlations for droplets entrainment fraction and the assumption where it equals zero are highlighted with marks.

Table 6 shows the average relative deviation $\bar{\epsilon}$ and its standard deviation σ_ϵ for the six different droplets entrainment fraction correlations and the two different sets of experimental data. Based on the calculated values, it is possible to compare the application of the different correlations in the numerical model.

Table 6. Average relative deviation $\bar{\epsilon}$ and its standard deviation σ_ϵ as a function of the six different droplets entrainment fraction equations and the two different sets of experimental data.

Data set	Deviations	$E_d = 0$	C1	C2	C3	C4	C5
Torres (1992)	$\bar{\epsilon}$ / [%]	54.32	51.61	30.50	47.38	45.65	46.02
	σ_ϵ / [%]	35.32	31.45	28.04	30.20	28.22	28.80
Aliyu *et al.* (2017)	$\bar{\epsilon}$ / [%]	69.81	67.15	90.05	62.82	60.17	60.64
	σ_ϵ / [%]	55.85	52.66	6.71	29.00	38.55	39.46

In general, the numerical model showed more agreement with experimental data from Torres (1992) than data from Aliyu *et al.* (2017). By analyzing the average relative deviations $\bar{\epsilon}$ and their standard deviations σ_ϵ, it is noticeable that, against data from Torres (1992), correlation C2 from Oliemans *et al.* (1986) showed the lowest values: $\bar{\epsilon} = 30.50\%$ and $\sigma_\epsilon = 28.04\%$. The assumption were E_d equals zero shows the highest deviations: $\bar{\epsilon} = 54.32\%$ with $\sigma_\epsilon = 35.32\%$.

Against the Aliyu *et al.* (2017) data, correlation C4 from Sawant *et al.* (2008) presented the lowest values, them being $\bar{\epsilon} = 60.17\%$ and $\sigma_\epsilon = 38.55\%$. The system adopted by Sawant *et al.* (2008) was also a vertical pipe, however, with 9.4 mm of internal diameter, it was almost 10 times smaller than the diameter used by Aliyu *et al.* (2017). The highest deviations were exhibited by correlation C2 from Oliemans *et al.* (1986): $\bar{\epsilon} = 90.05\%$ with $\sigma_\epsilon = 6.71\%$. Correlation C2 showed more agreement with experimental data from Torres (1992) although the correlation was developed for vertical pipes while its experiments were conducted in horizontal pipes.

One relevant aspect of the two data sets used for comparison concerns the internal diameter of the pipes. Torres (1992) used $D = 38.1$ mm and Aliyu *et al.* (2017) used $D = 101.6$ mm. The latter state that, although there are many correlations to predict the interfacial friction factor C_{fi}, hence the film thickness δ_f, the diameter range for validity of these correlations are generally restricted from 10 mm to 50 mm. This fact may explain the higher agreement with experimental data from the lower pipe diameter of 38.1 mm instead of 101.6 mm diameter. The number of points are distributed differently for both cases. The measured variation for Aliyu *et al.* (2017) is considerably smaller and all the δ_f with measured values are located between 0.007 and 0.013. At the same time, Torres (1992) had δ_f from 0.013 up to 0.244. These different ranges explains why the data is much more concentrated on Aliyu *et al.* (2017) results. Furthermore, is noticeable that the correlations used for the droplets entrainment fraction are valid for a small range with specific operational conditions and frequently shows inaccuracies with real results, especially in different conditions. That would also explain the results difference between Torres (1992) and Aliyu *et al.* (2017). Also the correlation depends on variables as velocity and diameter, that are different between both experiments.

5. CONCLUSIONS

This work presents a numerical model for calculating the film thickness in separated gas-liquid flows: horizontal stratified and vertical annular patterns. A comparative analysis of the proposed model and two sets of experimental data from the literature was conducted, in which the comparative parameters were the average relative deviations and their standard deviations. Also, five correlations for the droplets entrainment fraction, selected from the literature, were presented to be used in the numerical model, and their influence on the experimental data fitting was also analyzed.

The results showed more agreement with experimental data obtained for horizontal stratified flow (Torres, 1992) than vertical annular flow (Aliyu *et al.*, 2017). For stratified flow, the average relative deviation between calculated and measured film thickness was the lowest (30.50%) when the droplets entrainment fraction correlation by Oliemans *et al.* (1986) was used, while the highest relative deviation valued 54.32%. For annular flow, the lowest average relative deviation was 60.17% when using correlation by Sawant *et al.* (2008), while the value was 90.05%.

A possible explanation for the lower agreement with the annular flow data is the fact that correlations for estimating the interfacial friction factor are generally restricted from 10 mm to 50 mm internal diameter pipes, while experiments by (Aliyu *et al.*, 2017) were conducted in a 101.6 mm diameter tube. The correlations used to estimate the droplets entrainment fraction, which is dependent on several flow parameters such as gas-liquid ratio, may also be a source of deviation between calculated and measured values. Other than that, the determination of the shear stresses exerted by both the gaseous core and the liquid film on the pipe walls may also carry uncertainties, mainly due to the roughness of the pipes.

For future works, more correlations of interfacial friction factor and droplets entrainment fraction ought to be analyzed. The impact of pipe roughness and wall shear stresses could also be investigated. Furthermore, more experimental data sets should be compared against the numerical model.

6. ACKNOWLEDGEMENTS

The authors thank the Fundação Araucária (FA) for the scholarship awarded to Vinicius Sylvestre Simm, the Coordination for the Improvement of Higher Education Personnel (CAPES) for the scholarship awarded to Luiz Eduardo Muzzo, and the Federal University of Technology—Paraná—for the support received for the development of this work and the participation in this event.

7. REFERENCES

Aliyu, A.M., Baba, Y.D., Lao, L., Yeung, H. and Chun Kim, K., 2017. "Interfacial friction in upward annular gas–liquid two-phase flow in pipes". *Experimental Thermal and Fluid Science*, Vol. 84, pp. 90–109. ISSN 0894-1777. DOI 10.1016/j.expthermflusci.2017.02.006.

Cohen, L.S. and Hanratty, T.J., 1968. "Effect of waves at a gas-liquid interface on a turbulent air flow". *Journal of Fluid Mechanics*, Vol. 31, No. 3, pp. 467–479. ISSN 0022-1120. DOI 10.1017/s0022112068000285.

Haaland, S.E., 1983. "Simple and explicit formulas for the friction factor in turbulent pipe flow". *Journal of Fluids Engineering*, Vol. 105, No. 1, pp. 89–90. ISSN 0098-2202. DOI 10.1115/1.3240948.

Hanratty, T.J., 1991. "Separated flow modelling and interfacial transport phenomena". *Applied Scientific Research*, Vol. 48, No. 3-4, pp. 353–390. ISSN 1573-1987. DOI 10.1007/bf02008206.

Hart, J., Hamersma, P.J. and Fortuin, J.M.H., 1989. "Correlations predicting frictional pressure drop and liquid holdup during horizontal gas-liquid pipe flow with a small liquid holdup". *International Journal of Multiphase Flow*, Vol. 15, No. 6, pp. 947–964. ISSN 0301-9322. DOI 10.1016/0301-9322(89)90023-2.

Ishii, M. and Mishima, K., 1989. "Droplet entrainment correlation in annular two-phase flow". *International Journal of Heat and Mass Transfer*, Vol. 32, No. 10, pp. 1835–1846. ISSN 0017-9310. DOI 10.1016/0017-9310(89)90155-5.

Li, H., Wong, T.N., Skote, M. and Duan, F., 2013. "A simple model for predicting the pressure drop and film thickness of non-Newtonian annular flows in horizontal pipes". *Chemical Engineering Science*, Vol. 102, pp. 121–128. ISSN 0009-2509. DOI 10.1016/j.ces.2013.07.046.

Lima, L.E.M., 2011. *Análise do modelo de mistura aplicado em escoamentos isotérmicos gás-líquido*. Ph.D. thesis, Faculdade de Engenharia Mecânica, Universidade Estadual de Campinas, Campinas, SP, Brazil. URL `http://repositorio.unicamp.br/jspui/handle/REPOSIP/264105`.

Oliemans, R.V.A., Pots, B.F.M. and Trompé, N., 1986. "Modelling of annular dispersed two-phase flow in vertical pipes". *International Journal of Multiphase Flow*, Vol. 12, No. 5, pp. 711–732. ISSN 0301-9322. DOI 10.1016/0301-9322(86)90047-9.

Pedras, M.H.J., 1993. *Atrito interfacial em escoamento anular transicional*. Master's thesis, Faculdade de Engenharia Mecânica, Universidade Estadual de Campinas, Campinas, SP, Brazil. URL `http://repositorio.unicamp.br/jspui/handle/REPOSIP/264126`.

Sawant, P., Ishii, M. and Mori, M., 2008. "Droplet entrainment correlation in vertical upward co-current annular two-phase flow". *Nuclear Engineering and Design*, Vol. 238, No. 6, pp. 1342–1352. ISSN 0029-5493. DOI 10.1016/j.nucengdes.2007.10.005.

Sawant, P., Ishii, M. and Mori, M., 2009. "Prediction of amount of entrained droplets in vertical annular two-phase flow". *International Journal of Heat and Fluid Flow*, Vol. 30, No. 4, pp. 715–728. ISSN 0142-727X. DOI 10.1016/j.ijheatfluidflow.2009.03.003.

Torres, F.R., 1992. *Caracterização da interface e determinação experimental do fator de atrito interfacial em escoamentos horizontais estratificados*. Master's thesis, Faculdade de Engenharia Mecânica, Universidade Estadual de Campinas, Campinas, SP, Brazil. URL `http://repositorio.unicamp.br/jspui/handle/REPOSIP/264084`.

Wallis, G.B., 1969. *One-dimensional two-phase flow*. McGraw-Hill, New York, NY, USA. ISBN 9780070679429.

8. RESPONSIBILITY NOTICE

The authors are solely responsible for the printed material included in this paper.